PEAK FIELDS OF Nb$_3$Sn SUPERCONDUCTING UNDULATORS AND A SCALING LAW*

S.H. Kim[†]

Advanced Photon Source, Argonne National Laboratory
9700 S. Cass Ave., Argonne, IL 60439, USA

Abstract

The peak fields on the beam axis and the coil maximum fields of Nb$_3$Sn superconducting undulators (SCUs) were computed for a period length of 16 mm. The peak fields at the critical current densities were then calculated for a period range of 8 – 32 mm by using the scaling law for SCUs. Modification of Nb$_3$Sn strands increases the feasible peak fields of Nb$_3$Sn SCUs. To achieve this: 1) by reducing the superconducting filament size, the flux-jump instabilities at low fields must be prevented; 2) the conductor packing factor in the coil must be increased to about 0.8 by modifying the strand to a rectangular cross section and by reducing the insulation thickness. The achievable peak fields at $0.8J_c$ for Nb$_3$Sn SCUs then increase by more than 60% compared to those for NbTi SCUs.

INTRODUCTION

The peak field on the electron beam axis of a short-period undulator is one of the most important parameters for free-electron lasers and synchrotron radiation sources. In the recent years, superconducting undulators (SCUs), mainly using NbTi superconducting (SC) strands, are under development to achieve higher peak fields than those of permanent-magnet undulators [1-6]. A 22-period NbTi SCU was routinely charged up to near the critical current density for stability tests [7]. More recently, a 100-period NbTi SCU has been installed at the ANKA storage ring and operated with a gap of 8 mm [8].

Since the transition temperature T_c, the upper critical field B_{c2} and the critical current densities for Nb$_3$Sn SC strands are all higher than those for NbTi ones, one may expect to reach a higher peak field for an SCU with Nb$_3$Sn strands than for a NbTi SCU. Generally, an SCU requires a high packing factor for the coil winding and a low Cu/non-Cu ratio for the strand, which results in an adiabatic SC device. Under the adiabatic condition, the enthalpy, which is the heat capacity integral between the operating and current sharing temperatures, may play an important role in increasing the stability margin to accept the heat loads from the electron beam currents. This would, of course, depend on the design of the beam chamber and the interface between the chamber and the SCU. A Nb$_3$Sn SCU at 4.2 K operation has a higher enthalpy as compared to a NbTi SCU. A NbTi SCU at 1.8 K operation will increase the peak field. The enthalpy,

however, will be significantly reduced.

In spite of technical difficulties for developing Nb$_3$Sn coils, primarily due to the required heat treatments and brittleness of the strands, R&D efforts for Nb$_3$Sn SCUs have commenced [9, 10]. The achieved quench current densities were well below the expected critical current densities, mainly because of the flux-jump instabilities at low fields [11].

In this paper, achievable or feasible peak fields were calculated on the basis of commercially available Nb$_3$Sn SC strands and potential modifications of them. In the following section, the peak fields and coil maximum fields are computed for an undulator period of 16 mm and a gap/period ratio of 0.5. Then, the scaling law is introduced for Nb$_3$Sn SCUs [12]. Using the scaling law, the achievable peak fields and corresponding critical current densities are calculated for a period range of 8 - 32 mm, and the conclusion is presented in the last section.

FIELD CALCULATIONS

Figure 1 is a 2-D schematic of an infinitely long planar SCU cross section. The SCU has a period length λ along the z-axis and a pole gap of g. The coils have a dimension of (a x b) and current densities of $+J$ or $–J$. The upper and lower units of the SCU are symmetrical with respect to the z-axis. When the yoke is reasonably thick enough, the outer (top and bottom) coil windings do not directly contribute to the magnetic field distribution in the pole-gap region. The outer windings exist only for the SC wire transitions to the adjacent grooves and continuous winding of the coil [5].
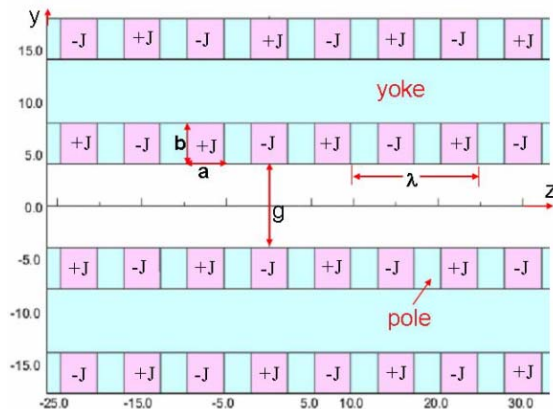

Fig. 1. A 2-D schematic of an infinitely long planar SCU in the yz-plane. The SCU has a period length λ along the z-axis, a pole gap of g, and a coil dimension of (a x b).

The vertical peak fields B_0 on the z-axis of a 2-D SCU were computed for a period length of 16, a pole-gap of 8, and five coil dimensions of (a x b), all in mm units, and are plotted as a function of the coil current density J in Fig. 2. The $B(H)$ data of low-carbon steel for the poles and yokes were used for the calculations. Figure 3 plots the corresponding coil maximum fields B_m. The critical current density J_c for the Nb_3Sn coil at B_m, also plotted in Fig. 3, limits the highest B_0 and B_m. For the selected five coil dimensions, see that the range of J_c is approximately within 1.8 – 2.2 kA/mm^2.
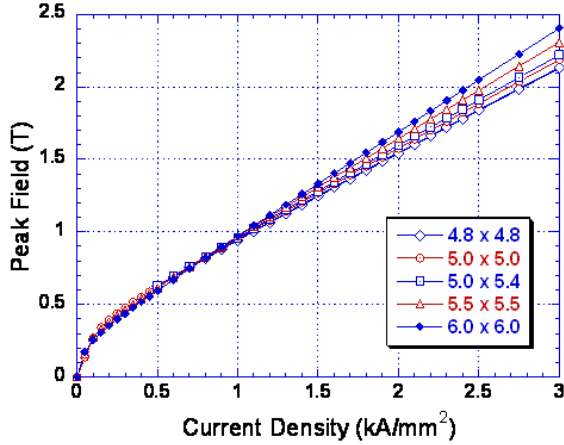

Fig. 2. The vertical peak fields B_0 on the beam axis as a function of the coil current density J for $\lambda = 16$ mm, $g/\lambda = 0.5$, and five coil dimensions.
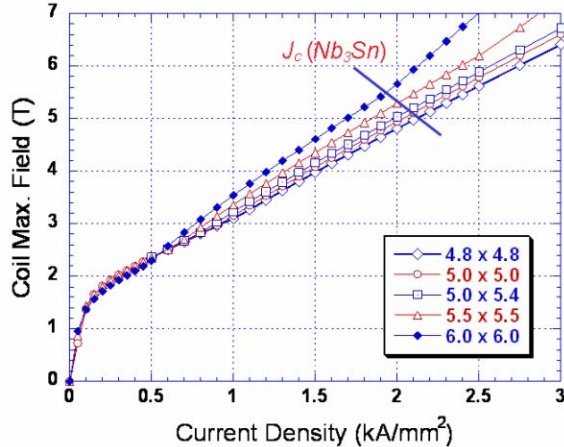

Fig. 3. The coil maximum fields B_m, corresponding the peak fields B_0 in Fig. 2, and the critical current density J_c for the Nb_3Sn coil.

THE SCALING LAW

When the dimensions of a SCU with a constant $J\lambda$ are scaled according to a period ratio, distributions of the magnetic field B and the magnetic permeability μ, as well as the B_0 and B_m, remain unchanged [12]. In addition, the dependence of the peak field on the pole gap g is approximately given by $exp(-\pi g/\lambda)$ for $g/\lambda > 0.2$. The maximum fields B_m, on the other hand, increase only

about 3% from infinity to $g/\lambda = 0.2$, greatly simplifying the scaling law and relevant calculations.

In order to show the gap dependence of the fields, the data for the (5.0 x 5.0) coil in Figs. 2 and 3 are plotted again in Fig. 4 with additional computed data for the pole gaps of 7 mm and 9 mm. As stated above, the B_m and J_c for the three pole gaps are approximately independent of the pole gap.
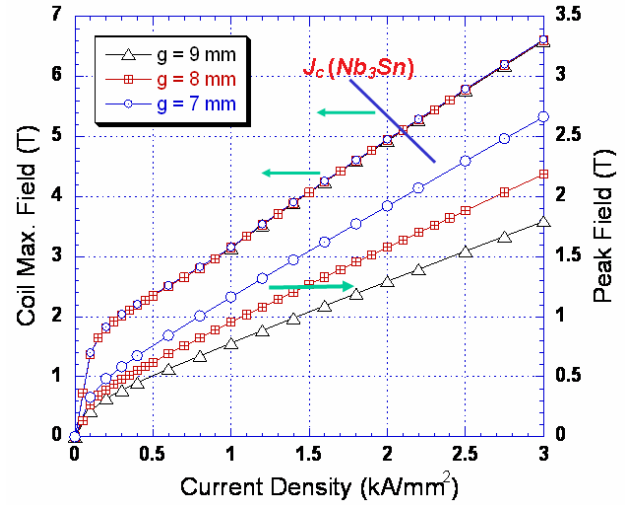

Fig. 4. The computed coil maximum field (*left axis*) and peak field (*right axis*) for $\lambda = 16$ mm and three pole-gaps. Also the critical current density $J_c(Nb_3Sn)$ (*bottom axis*) as a function of the SC coil B_m (*left axis*) at 4.2 K.

The empirical model of the field-dependent J_c for a Nb_3Sn strand at 4.2 K, without any strain effects, may use the following relation [13]:

$$J_c \, (kA/mm^2) = pf \, 2.8 \, (B_{c2}/B_m)^{0.5}(1 - B_m/B_{c2})^2, \qquad (1)$$

where pf is the packing factor of the bare SC strand in the coil, which depends on the coil design. Also, 21.4 T is used for the upper critical field B_{c2} at 4.2 K. For a packing factor of unity, J_c at 12 T was assumed to be about 1 kA/mm^2 [14, 15]. A pf of 0.56 is used for Eq. (1), as well as for the J_c curves in Figs. 3 and 4.

As seen from Figs. 2 and 3, a larger coil dimension gives generally a higher B_0 and B_m at a given current density. Least square fits of the (5.0 x 5.0) coil data sets of B_m and B_0 may be expressed as

$$B_m = 1.476 + 1.7234 \, J_n, \qquad (2)$$

and

$$B_0 = 0.343 + 0.6167 \, J_n, \qquad (3)$$

for $g/\lambda = 0.5$ and $(0.7 < J_n < 3.0)$. Here J_n is the reference current density for an arbitrarily chosen reference period $\lambda_n = 16$ mm. From Eqs. (1) – (3), J_c, the highest B_m at J_c, and B_0 at J_c, $0.8J_c$, $0.7J_c$ and $0.6J_c$ were calculated. Since B_0 varies approximately as a function of $exp(-\pi g/\lambda)$, all B_0 were calculated at $g/\lambda = 0.5$ in the remaining parts of this paper. It should be noted that the least-square fits,

corresponding to Eqs. (2) and (3), for the coils other than the (5.0 x 5.0) coil are not listed here.

Calculations of the peak field at a period λ other than at λ_n may be extended using the following relation:

$$J_n = J\lambda/\lambda_n. \qquad (4)$$

ACHIEVABLE PEAK FIELD

Using the scaling law in the previous section, the coil maximum fields B_m and the critical current densities J_c at B_m were calculated and are plotted for the period λ from 8 mm to 32 mm in Fig. 5. The coil dimensions in the inset key in the figure are those for $\lambda = 16$, all in mm units. As seen in the figure, among the selected coil dimensions, a larger coil generally gives a higher B_m, resulting in a lower J_c.

The peak fields at J_c in Fig. 5 and at fractions of J_c are plotted in Fig. 6. The spread of B_0 at a given period is much smaller than that of J_c and B_m shown in Fig. 5. And, except for the (6.0 x 6.0) coil, the dependence of B_0 on the coil dimension is almost negligible.
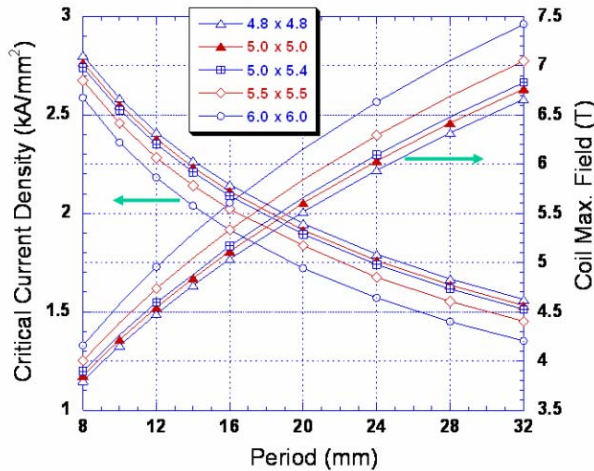

Fig. 5. The coil maximum fields B_m (*right axis*) and the corresponding critical current densities J_c (*left axis*) for undulator periods from 8 mm to 32 mm and $g/\lambda = 0.5$. The five coil dimensions in the inset key are for $\lambda_n = 16$ mm.

From the test results of a 22-period NbTi SCU, the achieved peak fields at $0.8J_c$ and near the J_c are shown as the data points of an open square and a filled square, respectively, at $\lambda = 14.5$ mm in Fig. 6 [7]. The circle data point at the same period comes from the test results of a Nb$_3$Sn SCU with a few-periods length [10]. The reason that the data point is lower than those calculated for $0.7J_c$ is believed to be due to the flux-jump instabilities for a strand of larger filament sizes at low fields [15]. The filament diameter was estimated to be about 80 μm for the Nb$_3$Sn strand diameter of 0.8 mm.

The NbTi coil had a packing factor higher than 0.8 by using rectangular SC wires with 25-μm-thick kapton insulation [5]. Even after further improvement of the

current density for a NbTi SCU by reducing the Cu/SC ratio and by increasing the J_c, the operating current density is unlikely to be higher than the data of $0.6J_c$ for Nb$_3$Sn SCUs in Fig. 6. The packing factor for the tested Nb$_3$Sn SCU was only about 0.56 by using SC strands with a diameter of 0.8 mm [10]. The same packing factor was used for the calculations of the data in Figs. 5 and 6. There are two reasons for this relatively low packing factor: Nb$_3$Sn strands use glass-woven insulation with thickness over 60 μm, and only round strands are commercially available.
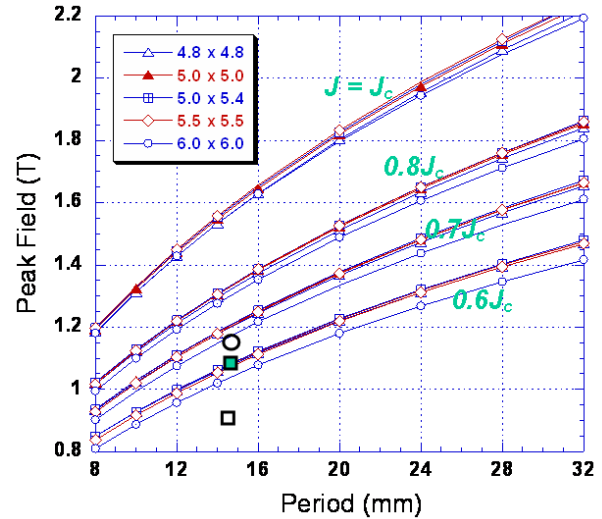

Fig. 6. The peak fields B_0 at $g/\lambda = 0.5$ for the J_c, corresponding to the data in Fig. 5, and their fractions. Two square data points come from the test results of a 22-period NbTi SCU at $0.8J_c$ and near the J_c. The circle data point comes from the test results of a Nb$_3$Sn SCU.

If Nb$_3$Sn strands are modified to have a rectangular cross section with a reduced insulation thickness of about 25 μm, the packing factor would be higher than 0.8. In Fig. 7, coil maximum fields and the corresponding critical current densities, calculated for $pf = 0.8$ and (5.0 x 5.0) coil, are plotted including those for $pf = 0.56$ in Fig. 5. Figure 8 compares B_0 for the two packing factors at J_c and $0.8J_c$. The new peak fields at $0.8J_c$ for $pf = 0.8$, for example, are as high as those at J_c for $pf = 0.56$. Two data points, approximately 0.95 T and 1.55 T at $\lambda = 14.5$ mm, compare the peak fields for a NbTi SCU and Nb$_3$Sn SCU, respectively, for $0.8J_c$ and $pf = 0.8$. The differences are more than 60%.

CONCLUSION

Modification of Nb$_3$Sn strands would increase the achievable peak fields of Nb$_3$Sn SCUs: First, by reducing the effective diameter of the SC filaments within the Nb$_3$Sn strand, the flux-jump instabilities at low fields must be prevented. For 0.8-mm strands, for example, a filament size less than 40 μm may be required. Second, the conductor packing factor in the coil winding must be

increased from the currently achievable 0.57 to 0.8. This requires a rectangular strand cross section. At the same time, the insulation thickness of the strand must be reduced to about 25 μm. At $0.8 J_c$, the achievable peak fields for Nb_3Sn SCUs would then be increased by more than 60%, compared to those for NbTi SCUs.
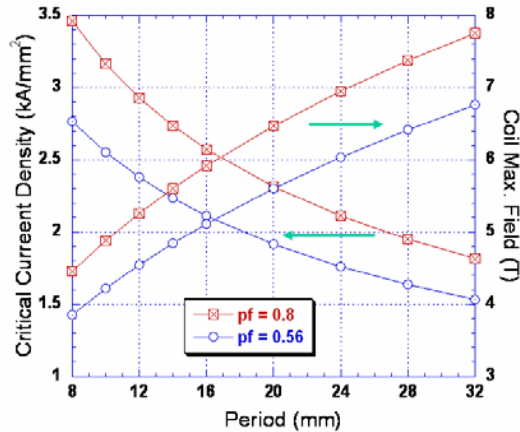

Fig. 7. The coil maximum fields (*right axis*) and the corresponding critical current densities (*left axis*), calculated for *pf* = 0.8 and (5.0 x 5.0) coil at $g/\lambda = 0.5$, are compared with those for *pf* = 0.56.
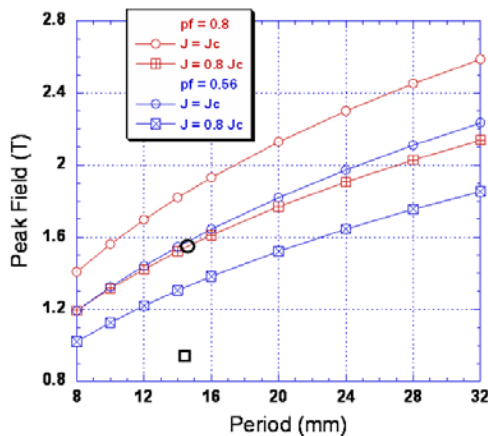

Fig. 8. The peak fields at J_c and $0.8 J_c$, corresponding to Fig.7, for packing factors, 0.8 and 0.56. Two data points at λ = 14.5 mm are the peak fields for a NbTi SCU and Nb_3Sn SCU, respectively, for $0.8 J_c$ and *pf* = 0.8.

REFERENCES

[1] I. Ben-Zvi et al., Nucl. Instr. and Meth A 297 (1990) 301; G. Ingold et al., *ibid*. 375 (1996) 451.

[2] T. Hezel et al., "Experimental Results with a Novel Superconductive In-Vacuum Mini-Undulator Test Device at the Mainz Microtron MAMI," Proc. of the PAC'99, New York City, March 1999, p. 165.

[3] A. Geisler et al., IEEE Trans. Appl. Supercond. Vol. 13 (2003) 1217.

[4] R. Rossmanith et al., "Superconductive 14 mm Period Undulators for Single Pass Accelerators (FELs) and Storage Rings," Proc. of the EPAC'02, Paris, June 2002, p. 2628.

[5] S.H. Kim et al., "Experimental Study of the Stability Margin with Beam Heating in a Short-Period Superconducting Undulators for the APS," Proc. of the EPAC'04, Lucerne, July 2004, p. 470.

[6] A. Hobl et al., IEEE Trans. Appl. Supercond. Vol. 15 (2005) 1232.

[7] S.H. Kim et al., *ibid*. 15 (2005) 1240.

[8] B. Kostka et al., "Operation of the ANKA Synchrotron Light Source with Superconducting Undulators," PAC 2005, Knoxville, Tennessee, May 2005; R. Rossmanith, private communication.

[9] S.O. Prestemon et al., IEEE Trans. Appl. Supercond. Vol. 15 (2005) 1236.

[10] S.H. Kim et al., "R&D of Short-Period NbTi and Nb_3Sn superonducting Undulators for the APS," PAC 2005, Knoxville, Tennessee, May 2005.

[11] C.P. Bean, Phys. Rev. Lett. 8 (1962) 250; Martin N. Wilson, *Superconducting Magnets*, Clarendon Press Oxford, 1983.

[12] S.H. Kim, Nucl. Instr. and Meth A 546 (2005) 604.

[13] L.T. Summers et al., IEEE Trans. Magn Mag-27 (1991) 2041.

[14] See, for example, E. Barzi et al., IEEE Trans. Appl. Supercond. Vol. 11 (2001) 3595.

[15] See, for example, E. Barzi, "Instabilities in Transport Current and Magnetization Measurements of Nb_3Sn and NbTi Strands," Workshop on Instabilities in Nb_3Sn Strands, Cables and Magnets," April 28-30, 2004, Fermilab, Batavia, IL.